Energetic electron (>10 keV) microburst precipitation, ~5–15 s X-ray pulsations, chorus, and wave-particle interactions: A review

Bruce T. Tsurutani,[1] Gurbax S. Lakhina,[2] and Olga P. Verkhoglyadova[1]

Received 6 November 2012; revised 27 March 2013; accepted 4 April 2013; published 28 May 2013.

[1] The fundamental features of ~0.1–0.2 s duration ~0.5 s spaced ionospheric electron precipitation "microbursts," ~5 to 15 s microburst "trains," and 5–15 s electron precipitation pulsations are reviewed in light of similar temporal structures of electromagnetic whistler mode "chorus" waves detected in the outer magnetosphere. Past observations of microbursts point to extremely rapid (ms timescale) wave-particle interactions, probably between lower band chorus subelements (durations of ~10 to 100 ms) and energetic ~10 to 100 keV electrons. A recent theory explaining such rapid interaction rates observed in microbursts is briefly reviewed. Arguments are given why ~5–15 s X-ray (and optical) pulsations are also associated with chorus scattering of energetic electrons. Comments about relativistic (E > 1 MeV) microbursts are also provided. There are, however, many other unsolved problems of outer zone energetic electron precipitation. The authors will attempt to indicate several of these for the interested reader. Finally, an appendix is provided for a brief review of two-frequency chorus and some current problems with that topic.

Citation: Tsurutani, B. T., G. S. Lakhina, and O. P. Verkhoglyadova (2013), Energetic electron (>10 keV) microburst precipitation, ~5–15 s X-ray pulsations, chorus, and wave-particle interactions: A review, *J. Geophys. Res. Space Physics*, *118*, 2296–2312, doi:10.1002/jgra.50264.

1. Introduction

1.1. Particle Precipitation

1.1.1. Microbursts and Microburst "Trains"

[2] Precipitation of energetic (~10–100 keV) outer zone radiation belt (outside the plasmasphere) electrons into the auroral ionosphere was first observed by balloon-borne bremsstrahlung X-ray detectors during magnetic storms [*Winckler et al*., 1958; *Anderson*, 1958; see also *Van Allen*, 1995]. It was soon determined from further high-altitude balloon flights that enhanced X-ray fluxes were associated with visible aurora and enhanced ground potentials [*Winckler et al*., 1959]. *Winckler et al*. [1962] were the first to record high temporal variations in the precipitating electron fluxes with ~0.1 s durations and ~0.5 s spacings, which *Anderson and Milton* [1964] in their work called "microbursts" (hereafter, designated as "μBs"). *Anderson and Milton* [1964] showed that some μBs occur as single events and some as multiple events. When μBs occurred in multiple groupings, they sometimes were spaced typically ~10 s apart [*Anderson and Milton*, 1964; *Barcus et al*., 1971]. These μB groupings were named "μB trains" (this name will be used hereafter in this paper). Using multiple balloons or multiple detectors on the same balloon payload, investigators determined that the scale size of the precipitation in the ionosphere (at a height of ~100 km) was ~100–150 km [*Brown et al*., 1965; *Parks*, 1967; *Rosenberg et al*., 1967]. μBs are mainly a daytime phenomenon occurring from late morning to early afternoon [*Anderson and Milton*, 1964; *Barcus et al*., 1966]. It should be mentioned that μBs sometimes also appear as long continuous trains for tens of minutes without apparent breaks in occurrence as well.

[3] *Brown et al*. [1965] detected μBs in the Northern Hemisphere (Fairbanks, Alaska) simultaneously with those in the Southern Hemisphere (MacQuarie Island, Australia) on approximately the same magnetic field lines. The authors suggested that plasma instabilities in the near-equatorial plane were responsible for the simultaneous precipitation in both hemispheres. *Rosenberg et al*. [1971], using the Siple Antarctica (L = 4.1) VLF ground receivers and balloon-borne X-ray detectors flown from the same location demonstrated the existence of a near time coherency between VLF waves and X-ray fluxes. This further solidified the idea that the energetic electron precipitation was due to a plasma instability located near the magnetic equator in which wave-particle interactions led to the scattering of the particles into the loss cone in both directions.

[4] *Lampton* [1967] made the first direct observation of the precipitating electrons from a rocket launched from Churchill, Manitoba, Canada. He reported the standard ~0.2 s μB durations and also noted that the electron fluxes for μBs appeared and disappeared within millisecond time scales. The ~60 keV electrons were delayed from ~90 keV

[1]Jet Propulsion Laboratory, California Institute of Technology, Pasadena, California, USA.
[2]Indian Institute of Geomagnetism, Navi Mumbai, India.

Corresponding author: B. T. Tsurutani, Jet Propulsion Laboratory, California Institute of Technology, Pasadena, CA 91109, USA. (bruce.tsurutani@jpl.nasa.gov)

2169-9380/13/10.1002/jgra.50264

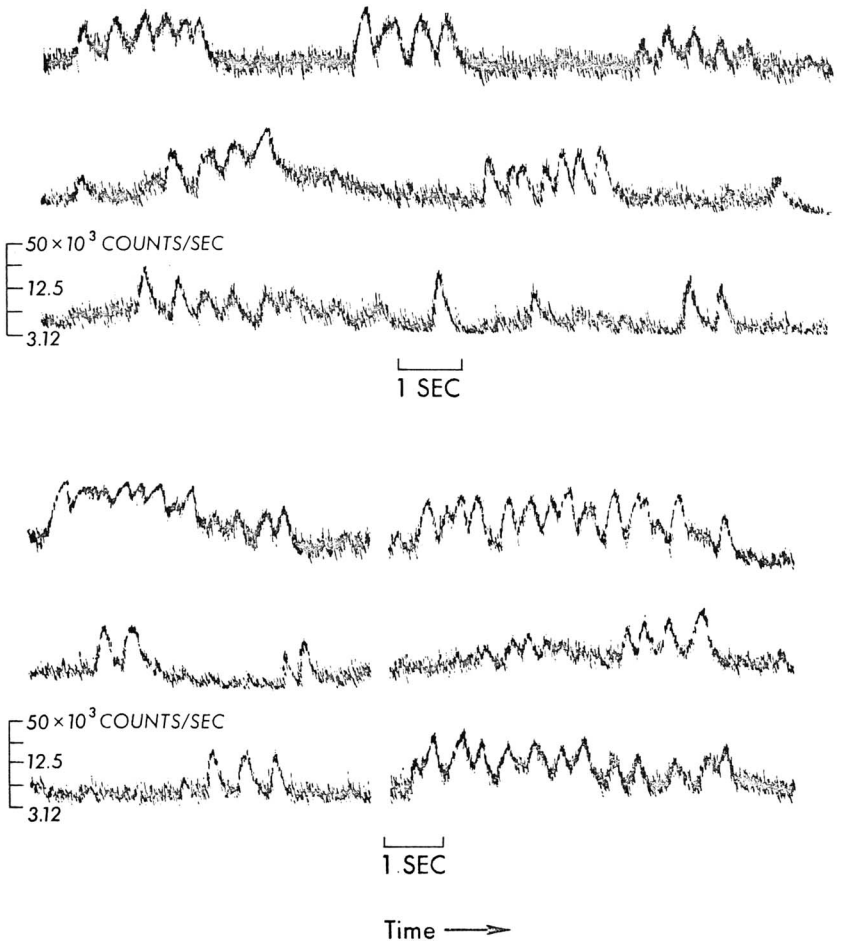

Figure 1. Samples of microburst bremsstrahlung X-rays detected from balloons flown at a height of 110,000 ft (~7 g/cm^2 atmosphere above the balloon) from Flin Flon, Manitoba, Canada, in 1962 and 1963 (a total of 15 flights). For scaling purposes, 1 s spacings are shown at the bottom of the third and sixth data panels. μBs occur as single events or in multiple events. The typical duration is ~0.2 s with separations of ~0.5 s (see the first, fourth, and sixth plots). Multiple μBs have been called "μB trains." Time separation between trains are ~10 s (see first and second panels). This figure was taken from *Anderson and Milton* [1964], their Figure 10.

electrons, implying a source high above the ionosphere (assuming all electrons had the same source and were pitch angle scattered at the same time). *Sandahl et al*. [1980] detected μB electron fluxes in a rocket flown over a pulsating aurora at Kiruna, Sweden. Although the particle detectors measured electron fluxes in the energy range from ~0 to 33 keV, μB modulation was only observable at energies above ~25 keV.

[5] Figure 1, taken from *Anderson and Milton* [1964], shows many of the μB features discussed above. Single and double event μBs can be noted in data plots 1, 2, and 4. Multiples or μB trains can be noted in data plots 1, 2, 4, and 6. The characteristic duration of μBs for these events are ~0.2 s with spacings of ~0.5 s. The spacings between the μB trains are ~10 s. The above are approximate numbers.

[6] The duration and shapes (rise and fall) of the individual μBs for the intervals in Figure 1 are quite similar. Different investigators studying different events have reported slightly different values for the μB durations, spacings, and μB train spacings. A μB event can last tens of minutes to hours.

1.1.2. Relativistic μBs

[7] *Imhof et al*. [1992] discovered >1 MeV loss cone electron flux enhancements with <1 s time scales by instrumentation on board the S81-1 low-altitude spacecraft. These events are called relativistic μBs. Most of the relativistic μBs occurred between L = 4 and 6 during intervals of enhanced geomagnetic activity. *Nakamura et al*. [2000] did a statistical survey of relativistic μBs using low-altitude Solar, Anomalou, and Magnetospheric Particle Explorer (SAMPEX) data. They found that relativistic μBs occurred preferentially during magnetic storms compared to nonstorm intervals and were detected in the ~3 to 9 magnetic local time (MLT) hours.

[8] *Lee et al*. [2012], using the STSAT-1 data, have shown that ~170 to 360 keV electron data at ~680 km altitude exhibited a two-component spectra. The precipitation component parallel to the ambient magnetic field lines were softer than the perpendicular (trapped) component. It was also noted that the loss cone was only partially filled.

[9] Relativistic μBs are considered to be important because they are thought to be a major source of loss of the relativistic electron content of the outer radiation belts [*Lorentzen et al*.,

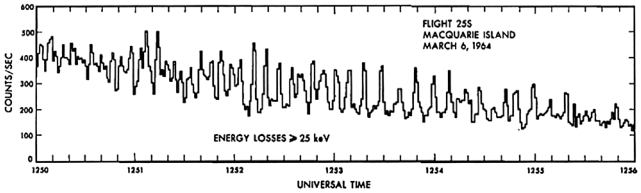

Figure 2. The ~5–15 s bremsstrahlung X-ray pulsations detected by balloon-borne detectors over MacQuarie Island, Australia, during a storm of 6 March 1964. This portion of the pulsation event occurred from 1250 to 1256 UT (~23 LT). This figure was taken from *Brown et al*. [1965], their Figure 10.

2001a, 2001b; *Horne and Thorne*, 2003; *Thorne et al*., 2005; *Bortnik and Thorne*, 2007; *Saito et al*., 2012]. However, whether chorus is the major wave mode responsible for the majority of relativistic electron loss or not has recently been debated [e.g., see *Horne and Thorne*, 1998].

1.1.3. X-Ray Pulsations

[10] X-ray pulsations (associated with 10–100 keV electron precipitation) were also detected by high-altitude balloon experiments but were noted to occur at a considerably different local time than μBs and μB trains. Pulsations were originally considered to be different from μB trains because there were no obvious rapid flux variations on the time scale of μBs present in the former. The first work reporting ~5–15 s pulsations in X-rays was *Anger et al*. [1963]. They reported a variable repetition rate with a quasi-period between ~1 and ~15 s. The mean time was ~8 s. *Brown et al*. [1965] observed simultaneous X-ray pulsations from Fairbanks, Alaska, and MacQuarie Island, Australia. No detailed correlation in either time or amplitude was found, however. This may have to do with the small-scale size of the precipitation regions in the ionosphere being ~100 km [*Brown et al*., 1965]. *Barcus et al*. [1966] and *Rosenberg et al*. [1967] both indicated that ~5–15 s pulsations occurred from ~midnight to ~dawn, in strong contrast to the local time dependence of μBs and μB trains (from ~dawn to ~postnoon). *Rosenberg et al*. [1967] noted that ~5–15 s pulsations occurred preferentially near the equatorial border of the auroral zone. *Brown et al*. [1965] noted that the scale size of pulsation precipitation is approximately the same as that for μBs.

[11] *Barcus and Christensen* [1965] have reported pulsations with periods of ~75 s. *Barcus and Rosenberg* [1965] have detected ~3 min and ~5 min X-ray pulsations in the late stages of magnetic storms. These longer-period X-ray pulsations are less common than ~5–15 s pulsations.

[12] Figure 2 shows examples of ~5–15 s X-ray pulsations occurring over MacQuarie Island, Australia, on 6 March 1964. The spacings between pulsation peaks varied between ~5 and ~12 s, with an average of ~8.6 s. The pulsations are quasi-periodic and occurred superposed on an elevated (above cosmic ray background) flux. Pulsations were also detected on a flight over Fairbanks, Alaska, at the same time, but coherent conjugate pulsations were not detected.

1.1.4. The ~5–15 s X-Ray Pulsation Relationship to ~5–15 s Optical Pulsations

[13] There are many types of auroral structures that pulsate in optical wavelengths [*Cresswell and Davis*, 1965]. The diffuse, irregularly shaped patches with scale sizes of ~50 km (type 5 in *Cresswell and Davis* [1965]) have been found to be correlated with X-ray pulsations [*Scourfield et al*., 1970]. The most common type of optical pulsations are small filamentary structures (tens of structures have been simultaneously viewed from a single ground observatory) that pulsate asynchronously [see also *Brekke*, 1971; *Oguti*, 1976]. It is not known if these smaller-scale structures have X-ray analogs or not. *Johansen and Omholt* [1966] have reported that they detected pulsations in all types of auroras. Optical pulsations occur after midnight and after substorm expansion phases. *Scourfield and Parsons* [1971] have documented the development of auroral optical pulses. There is a steady increase in one small spatial region, then a rapid expansion outward at speeds of ~25 to 250 km/s (at ~100 km altitude) until the full size of the pulsation patch has been attained.

[14] *Yamamoto* [1988] reported optical pulsations on the time scale of μBs (~3 Hz). He noted that the scale size of ~5–15 s pulsations are comparable to the gyroradius of a few tens of keV protons, or ~100 km in the ionosphere. *Yamamoto* [1988] noted that optical pulsation intensities have rapid on-off switching, not smooth sinusoidal variations. *Nishimura et al*. [2010] studied pulsations using the THEMIS satellites and all-sky ground-based visible imagers. They found that it is the lower frequency band of chorus [*Tsurutani and Smith*, 1974] that is driving optical pulsations. Using a two-THEMIS spacecraft technique, *Nishimura et al*. [2011] estimated the size of the optical patches in their study to be the same magnitude that *Yamamoto* [1988] determined, ~100 km.

[15] We direct the interested reader to *Yamamoto* [1988] and to *Li et al*. [2012a] and *Lessard* [2012] for recent reviews on optical pulsations and their relationship to electron precipitation.

1.1.5. Electron Precipitation Mechanisms

[16] Although many precipitation mechanisms were proposed after μBs, μB trains, and 5–15 s after pulsations were discovered, the sum total of the observations point to plasma instabilities generated in the equatorial plane of the magnetosphere. The first to discuss a Doppler-shifted cyclotron resonance mechanism between electromagnetic ELF-VLF waves and ~10–100 keV electrons in the magnetosphere was *Brice* [1963]. It is noted that for parallel propagating electromagnetic waves, the ratio of wave electric to magnetic component is $1/n << 1$, where n is the index of refraction. It is found that for low-frequency waves ($\omega^2 << \Omega^2$, where ω is the wave frequency and Ω the electron gyrofrequency), the electric component of the wave interacting with electrons produces a smaller pitch angle change compared to the magnetic component [*Inan et al*., 1978]. We note that at highly oblique wave propagation angles, the electric field component can be substantial, and its effect cannot be ignored [*Verkhoglyadova et al*., 2010]. For illustrative purposes and because chorus near the amplification region (the equator) is propagating primarily parallel to B_0, we will discuss only the particle interaction with the magnetic component of the electromagnetic waves. *Brice* [1964a] identified a temperature anisotropy/loss cone instability as the mechanism for VLF chorus growth (see also *Sudan* [1963] and *Bell and Buneman* [1964]). *Brice* [1964b] laid out the fundamental physics for energy transfer from the energetic electrons to the electromagnetic waves.

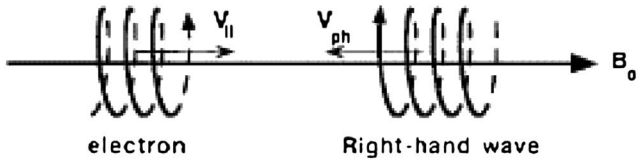

Figure 3. A schematic of a "normal" Doppler-shifted cyclotron resonance between an electron and a right-hand polarized electromagnetic wave. Taken from *Tsurutani and Lakhina* [1997], their Figure 8.

[17] *Kennel and Petschek* [1966] put the temperature anisotropy/loss cone instability into a full theoretical context, establishing a self-consistent expression for the pitch angle diffusion of electrons (and also protons). *Kennel and Petschek* [1966] assumed that the VLF waves amplified by the instability propagate away from the generation region (the magnetic equator), reflect, and then return to the equator for further interactions. This mechanism was developed assuming incoherent VLF waves. The derived expression for diffusion was not intended to explain the μB temporal structure, however.

[18] Figure 3 shows a schematic of the electron-wave cyclotron-resonant interaction. Electrons have a right-hand cyclotron motion about the ambient magnetic field, B_0. The expression for cyclotron resonance is as follows:

$$\omega - k_{\|} v_{\|} = n\Omega/\gamma \tag{1}$$

where ω is the wave frequency, $k_\|$ and $v_\|$ are the parallel (to B_0) components of the wave **k** vector and the particle velocity vector, **v**, respectively. Ω is the electron cyclotron frequency, n is the harmonic number integer (0,±1, ±2,...), and γ is the relativistic factor $(1 - v^2/c^2)^{-1/2}$. In the expression for γ, v is the particle speed, and c is the speed of light. For positive (negative) values of n, equation (1) represents the normal (anomalous) resonant condition. For normal (n = 1,2,...) Doppler-shifted cyclotron resonance, the waves and particles are traveling in opposite directions along the magnetic field as shown in Figure 3. The waves will be Doppler-shifted up to the electron cyclotron frequency or its harmonics. The more energetic the particles, the lower the frequency of the waves needed for resonance, and vice versa; the higher the wave frequency, the lower the parallel kinetic energy of the particles needed for resonance.

[19] For the fundamental normal electron cyclotron resonance (n = 1), the expression in (1) can be divided by $k_\|$ and thus be written in a slightly different way:

$$v\| = v_{\rm ph}[1 - \Omega/(\omega\,\gamma)] \tag{2}$$

Here v_{ph} is the parallel wave phase speed. From this expression, it can be noted that the lower the wave phase speed, the lower the speed of the resonant electrons. The higher the wave phase speed, the higher the parallel speed of the resonant electrons. We will come back to some of these points later in the paper.

[20] Figure 4 gives two examples of the pitch angle scattering mechanism that was discussed in *Brice* [1963, 1964b]. During cyclotron resonance between the electron and the wave, the particle senses the wave as a static field in phase with its gyromotion. In the left-hand panel, the parallel component of the electron velocity ($V_\|$) interacts with B_ω, giving the Lorentz force F_L. The electron is decelerated in V⊥. In this case, the particle pitch angle is decreased. If the phase of the wave was 180° from the present case (B_ω was directed downward), the Lorentz force would be in the opposite direction. For this case, both the electron perpendicular energy and its pitch angle would be increased.

[21] The right-hand panel shows that the Lorentz force F_L will accelerate the particle parallel velocity along B_0. If the phase of the wave is 180° opposite to that shown in the schematic, then the Lorentz force direction would be reversed, and the pitch angle changes would be opposite to that above.

[22] Using the above basic physics, the assumption of incoherent electromagnetic waves, and randomness in the wave-particle interaction phases, *Kennel and Petschek* [1966] derive the following pitch angle diffusion expression:

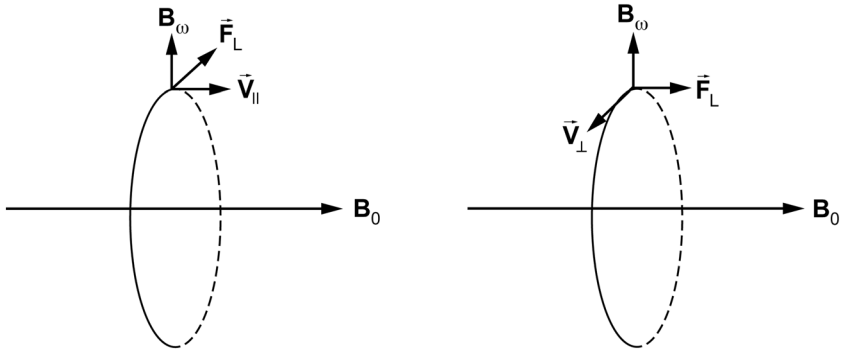

Figure 4. Pitch angle scattering of electrons by the magnetic component of transverse electromagnetic waves (B_ω). In the schematic, the waves are assumed to be propagating in an antiparallel direction relative to the ambient magnetic field, B_0. The electrons are gyrating about B_0 and propagating along B_0. Pitch angle scattering is due to the Lorentz force associated with the particle velocity component orthogonal to the wave magnetic field. The left-hand panel shows the case for the parallel component of the electron velocity vector ($V_\|$) and the right-hand panel the case for the perpendicular velocity component (V⊥). The figure is an adaptation from *Tsurutani and Lakhina* [1997], their Figure 12.

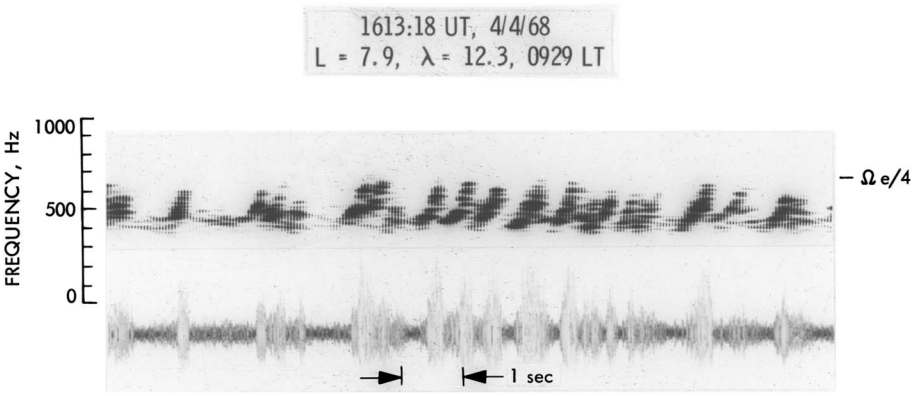

Figure 5. An example of dayside rising tone chorus. The tones often overlap each other. The data were taken from the searchcoil experiment onboard the OGO5 satellite.

$$D_{\alpha\alpha} = (\Delta\alpha)^2/2\Delta t = \left(\Omega^2/2\right)(B_\omega/B_0)^2\Delta t \qquad (3)$$

[23] In the above, $\Delta\alpha$ is the incremental change in pitch angle, and Δt the incremental time of interaction. The interaction time Δt will be discussed in more detail later in this paper. This expression was used to establish the upper limit of 10–100 keV electron flux in the outer magnetosphere.

1.1.6. Mechanism for μB Trains and 5–15 s Pulsations

[24] An early possible explanation for both μB trains and 5–15 s pulsations was ~5–15 s electromagnetic micropulsations modulating the electron loss cone/temperature anisotropy. *Coroniti and Kennel* [1970a] noted that X-ray pulsations occur during enhanced X-ray fluxes (see Figure 2 and *Brown et al*. [1965]) and suggested that the magnetic component of the micropulsations might thus modulate an already ongoing electron temperature anisotropy instability. Coroniti and Kennel produced a linear theory to explain the electron modulation. In a second work, *Coroniti and Kennel* [1970b] identified the sharp electron thermal gradient at the plasmasheet boundary as a source of free energy for an Alfvén wave drift instability. The fastest growing wave was shown to have a period of ~10 s, the observed period of the quasi-periodic pulsations. The authors noted at the time of their articles that such micropulsations had not been seen in the wave generation region (the equator) and that details of these waves would be needed to determine exactly how the temperature anisotropy/loss cone instability would be modulated.

[25] *Davidson* [1979] on the other hand proposed a self-modulation mechanism which also requires a marginally unstable energetic electron distribution (following *Brown et al*. [1965] and similar to *Coroniti and Kennel* [1970a]). Davidson's model has the pulsations being a consequence of growth of chorus and removal of trapped electrons following an electron injection event. If too many electrons are removed by wave-particle interactions, the system restores itself by building up the flux again to values exceeding the equilibrium flux.

2. Waves: Chorus Observations

[26] Chorus is an electromagnetic wave which propagates in the whistler mode (right-hand polarized relative to the ambient magnetic field direction B_0). The emissions were detected most prevalently at local dawn; thus, K.W. Tremellen (who worked for Marconi's Research Laboratories, Great Baddow, Essex, England) gave it the name "dawn chorus" because it sounded like a "dawn chorus of birds" [*Storey*, 1953; *Isted and Millington*, 1957]. Since the emission was detected at local times other than at dawn, the name was later shortened to just "chorus." The emissions have rising frequency-time structures, with durations ~0.2 s with spacings of ~0.5 s. It was immediately obvious to X-ray microburst researchers that chorus was the most likely plasma wave that was responsible for energetic electron pitch angle scattering and loss into the auroral ionosphere.

[27] The equatorial generation of chorus was confirmed by the first satellites that surveyed the equatorial region of the outer magnetosphere (outside the plasmasphere). *Gurnett and O'Brien* [1964], *Russell et al*. [1969], and *Burtis and Helliwell* [1969], explored these waves using the magnetospheric Injun 3, OGO-3 and OGO-1 satellites, respectively. Collectively, they found emissions to occur near the equator from $L \sim 5$ to $L \sim 10$ from ~midnight to ~1400 LT. More recently, researchers using Poynting flux measurements have placed the generation region to within ~1° of the magnetic equator [*LeDocq et al*., 1998; *Lauben et al*., 2002]. *Tsurutani and Smith* [1974, 1977], using OGO-5 satellite ELF wave data, determined that chorus was generated during substorms, explaining the delay of chorus from substorm onset by gradient and curvature drift of ~10–100 keV electrons from midnight to the local time of observation. Anisotropic ($T_\perp/T_\parallel > 1$) 79 keV electrons were found to be coincident with chorus [*Tsurutani et al*., 1979], as expected from the *Kennel and Petschek* [1966] loss cone/temperature anisotropy theory. The electron anisotropy is presumed to be associated with the compression of the electrons during strong convection/injection of the nightside plasma sheet during substorms [*DeForest and McIlwain*, 1971].

[28] Figure 5 gives an example of dayside chorus at ~0929 LT and $L = 7.9$. The chorus tones last ~0.3 s and are separated by ~0.5 s with some overlap between the high-frequency end and the low-frequency beginning of the next tone. All of the rising tones have essentially the same frequency-time shape. Different chorus events have different frequency-time shapes. The similarity of the duration of chorus tones and microbursts is quite obvious.

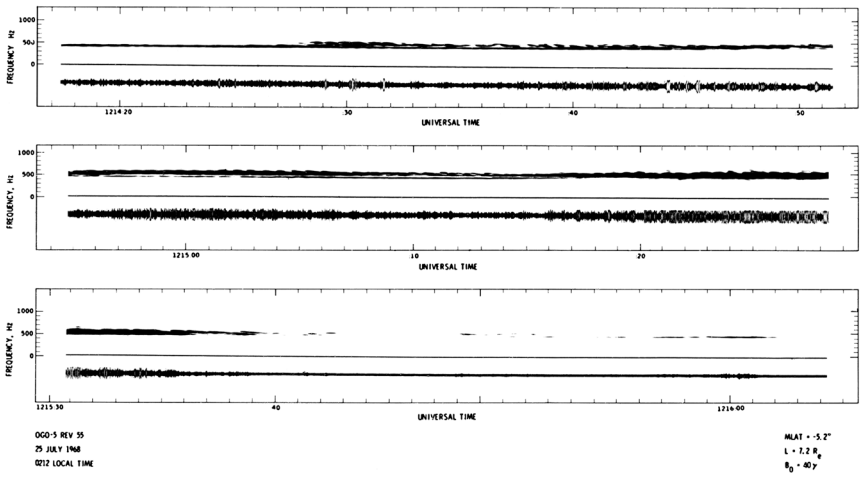

Figure 6. A time sequence of three panels showing flat/falling-tone chorus. The figure was taken from *Goldstein and Tsurutani* [1984], their Figure 10.

[29] The characteristic of chorus that occurs on the nightside (from midnight to dawn) is often considerably different than "dawn chorus" or dayside chorus. Nightside chorus is often composed of flat tones, falling tones, or even hiss-like signatures [*Tsurutani and Smith*, 1974; *Goldstein and Tsurutani*, 1984; *Hayakawa et al*., 1990]. Figures 6–8 show examples of these three types of chorus.

[30] The chorus shown in Figure 6 was detected by OGO-5 at ~0212 LT at L = 7.2. The waves were detected quite close to the equatorial generation region, −5.2° magnetic latitude (MLAT). Three panels of continuous data are shown. In the top panel, chorus starts as a simple tone, then evolves into falling tones or even "u-shaped" emissions, then into overlapping falling tones. All of these emissions occurred at frequencies below $\Omega_{eq}/2$, where Ω_{eq} is the electron cyclotron frequency at the magnetic equator.

[31] Figure 7 shows an example of ~5–15 s structureless hiss pulsations. The hiss can be seen in the inset as structureless emissions extending from ~300 to ~500 Hz (the gap at

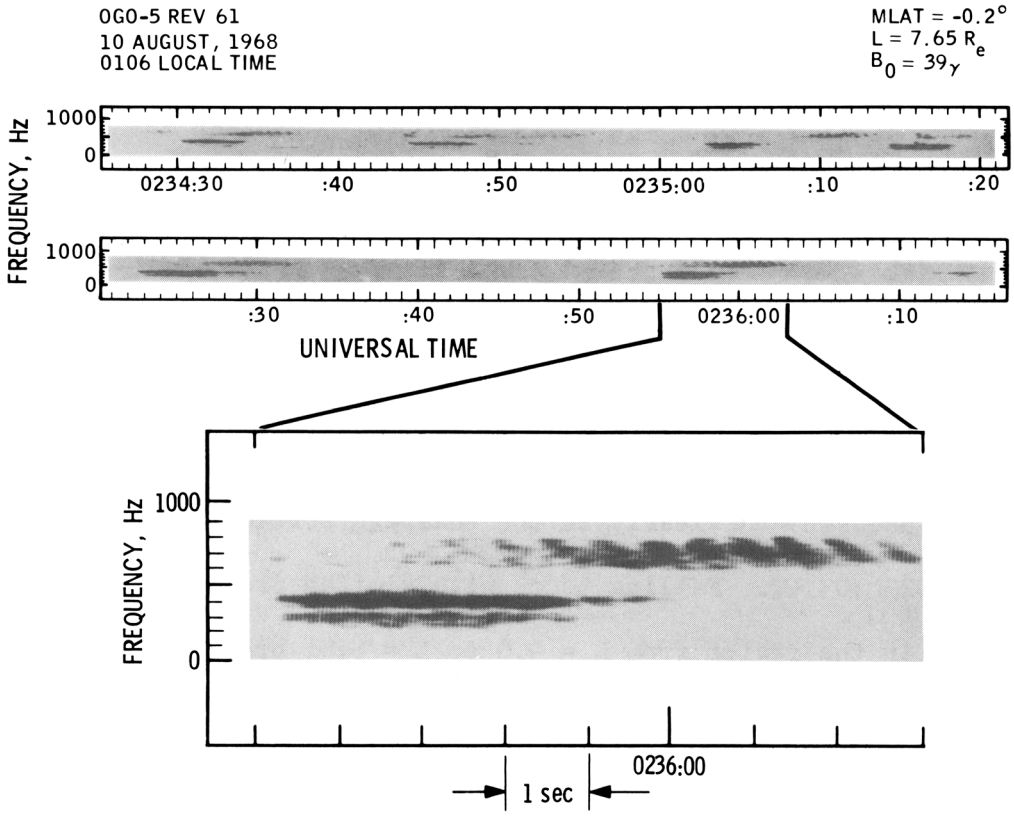

Figure 7. Hiss followed by overlapping falling-tone chorus. The hiss events were separated by 5–15 s intervals. Taken from *Tsurutani and Smith* [1974], their Figure 3.

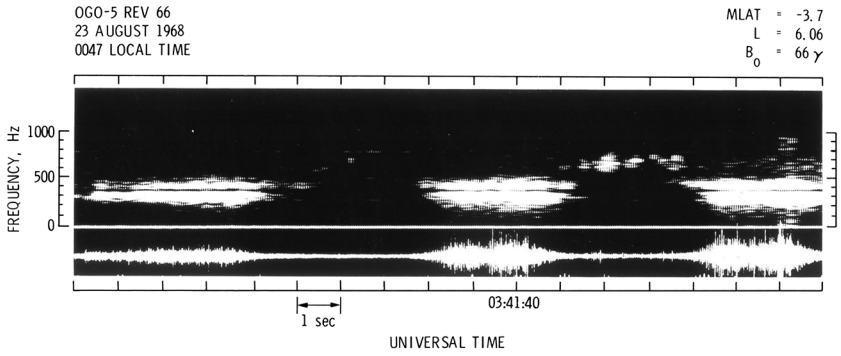

Figure 8. Quasi-periodic ~5 to 15 s hiss detected in the outer magnetosphere near local midnight (~0047 LT). Taken from *Goldstein and Tsurutani* [1984], their Figure 14.

~400 Hz should be ignored; it is an artifact created by a notch filter, used to take out a spacecraft interference tone). After each hiss burst, higher frequency overlapping chorus falling tones occur. These latter emissions are present from ~700 to ~850 Hz. Both the hiss and the falling-tone chorus recur at ~5 to 15 s quasi-periods. This event occurred at ~0106 LT at L = 7.7. The two types of chorus has been called two-frequency chorus, where the gap without emission has been found to be at ~0.5 Ω_{eq} [*Tsurutani and Smith*, 1974].

[32] *Tsurutani and Smith* [1974] reported that there were no in-phase magnetic pulsations at ~5 to 15 s quasi-periods associated with the hiss bursts, contrary to the expectations of the predictions from *Coroniti and Kennel* [1970a]. Other similar ~5 to 15 s pulsation events detected near the equatorial plane similarly did not have related micropulsations. *Oguti et al*. [1986] using GOES 2 and 3 satellite data also noted the lack of equatorial magnetic pulsations during ground auroral pulsations.

[33] Electromagnetic emissions without apparent temporal structure are also detected in the outer magnetosphere. Figure 8 shows an example of ~5–15 s electromagnetic hiss pulsations detected at L = 6.1 at a local time of ~0047 LT. The spacecraft at the time of wave detection was quite close to the magnetic equator (MLAT = −3.7°), but the emission was more or less structureless. There are higher frequency chorus emissions in the trailing part of the second pulse, shown in the middle of the data panel. Although this was a different event from the one shown in Figure 7, the hiss and following higher frequency emission are strikingly similar.

[34] We refer the reader to *Helliwell* [2006], Chapter 7 for a variety of chorus frequency-time shapes that have been detected by the Stanford University ground-based receivers. It is remarkable how many different types have been noted and recorded. See also *Li et al*. [2012b] for a discussion of hiss-like emissions and discrete chorus elements (both rising and falling tones) in the outer magnetosphere. The authors suggest that the ratio of plasma frequency to the electron gyrofrequency (Ω_{pe}/Ω) may play an important role in the form of the electromagnetic emission frequency-time structure. *Li et al*. [2012b] find that rising tone and falling-tone chorus are found primarily in regions of low Ω_{pe}/Ω values. They also find that falling tones propagate at oblique angles to the magnetic field, contrary to the examples shown in the above figures.

3. Electrons and Chorus

3.1. The Relationship Between μBs, μB Trains, Pulsations, and Chorus

[35] Chorus elements, chorus ~5–15 s trains, and ~5–15 s hiss pulsations have time scales quite similar to μBs, μB trains, and ~5–15 s X-ray pulsations. It seems likely that the waves are responsible for the pitch angle scattering of ~10 to 100 keV equatorial electrons into the loss cone, generating the ionospheric X-rays with similar time scales.

[36] The local time dependence of the frequency-time structure of chorus can help explain the frequency-time structure of the auroral zone electron precipitation. Although past observations indicate that overlapping falling tones, flat tones, hiss-like structures (Figures 6–8), and rising tones (Figure 5) can be detected at all local times, night or day, the observations of *Tsurutani and Smith* [1974], *Burtis and Helliwell* [1976], *Goldstein and Tsurutani* [1984], and *Hayakawa et al*. [1990] indicate that falling tones, flat tones, and hiss-like structures are detected primarily in the nightside sector prior to dawn, and rising tone chorus is detected in the postdawn time sector. It should be pointed out that the data used in the above chorus studies and also the μB, μB train, and X-ray pulsation studies were done in essentially the same phase of the solar cycle, near solar maximum.

[37] *Li et al*. [2011a] have done a statistical survey of chorus using the THEMIS wave data. They found falling tones to occur predominantly on the dayside. The *Li et al*. [2011a] data were taken from 1 June 2008 to 1 April 2011, an interval near an extended solar minimum (see *Tsurutani et al*. [2011a] for detailed discussion of the latter). Since these results are contrary to the bulk of past observations of chorus, we will assume that this may be a possible solar cycle effect and will not be addressed in our general explanation of the relationship between chorus and electron precipitation. More will be stated on this topic later in the paper.

[38] During time intervals near solar maximum, chorus tones occurring from midnight to near dawn have flat or overlapping falling-tone structures. Thus, electrons scattered into the loss cone by cyclotron resonance with these tones will lose any one-to-one correlation with each chorus element (if any) as the electrons propagate from the equatorial scattering region to the ionosphere. This can explain the lack of μB and μB train detection in this particular local time region.

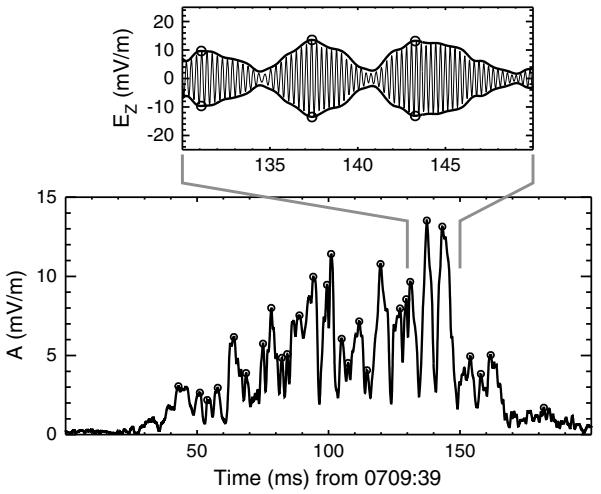

Figure 9. Wave amplitude variation within a ~0.1 s chorus element. The inset shows the electric field variation for several packets/subelements. The subelements have durations of ~30 ms. The Figure is taken from *Santolik et al*. [2004], their Figure 4.

[39] In the ~ dawn-to-postnoon local time sector, rising tone chorus dominates (Figure 5). Many of these cases have tones that are clearly separate from each other (see GEOTAIL examples in *Tsurutani et al*. [2009]). In these latter cases, rapid pitch angle scattering by these chorus elements would lead to distinct separate bursts of electron precipitation which could be detected as μBs at ionospheric heights.

[40] Although this explanation seems reasonable to explain the electron precipitation temporal structure, a fundamental question arises: "During solar maximum, why is the dayside dominated by falling-tone chorus?" We also have the converse question "During solar minimum, why is the dayside dominated by rising tone chorus?" At this time, we do not have concrete answers. *Nunn* [1974] and *Omura et al*. [2008] have attempted to model rising tone chorus, and *Nunn and Omura* [2012] have attempted to explain flat and falling-tone chorus. One fundamental difference between the solar wind during solar maximum and solar minimum is that during solar maximum, Interplanetary Coronal Mass Ejections (ICMEs) dominate solar activity causing large magnetic storms [*Gonzalez et al*., 1994], whereas during the last solar minimum, the solar wind was dominated by slow solar wind and exceptionally weak high-speed streams [*Tsurutani et al*., 2011a]. The latter could lead to a more extended magnetosphere (larger and less compressed on the dayside) than normal.

[41] Another difference between the dayside and nightside magnetosphere is the significantly higher thermal plasma densities in the dayside. Sunlight heating of the ionosphere (at dawn) can lead to an upwelling of thermal plasma into the outer magnetosphere [*Banks and Holzer*, 1968]. *Brice and Lucas* [1971] and *Jentsch* [1976] have invoked the presence of enhanced postdawn thermal plasma in the magnetosphere to cause a lowering of the resonant energetic electron energy and thus a strong growth of the electron temperature anisotropy/loss cone instability (assuming a power law electron energy distribution). This can explain the maximum of electron precipitation [*Hartz and Brice*, 1967] and magnetospheric chorus intensities [*Tsurutani and Smith*, 1977] at ~local dawn (thus the original name "dawn chorus"). This change in the thermal plasma condition may be related to the change in the nature of the chorus frequency-time structure as well. There are other differences in these two local time regions. On the dayside, the ambient magnetic field lines are flattened due to solar wind compression, while the nightside fields are elongated. A third factor is that electron temperature anisotropy will change its nature as a function of local time due to dispersion of the ~midnight injected substorm electrons by gradient and curvature drift and drift-shell splitting.

3.2. Chorus Wave Subelements and Wave Coherency

[42] *Santolik et al*. [2003, 2004] have shown that chorus elements from the Cluster dataset are composed of substructures that have the appearance of small packets. Figure 9 shows three such packets within a chorus element (tone). The chorus elements are ~0.1 s in duration, and the packets (hereafter called subelements) have durations of ~5 ms.

[43] Chorus subelements have recently been shown to be coherent waves [*Tsurutani et al*., 2009]. *Tsurutani et al*. [2011b] examined Polar chorus data and demonstrated that the two transverse axes of the circularly polarized

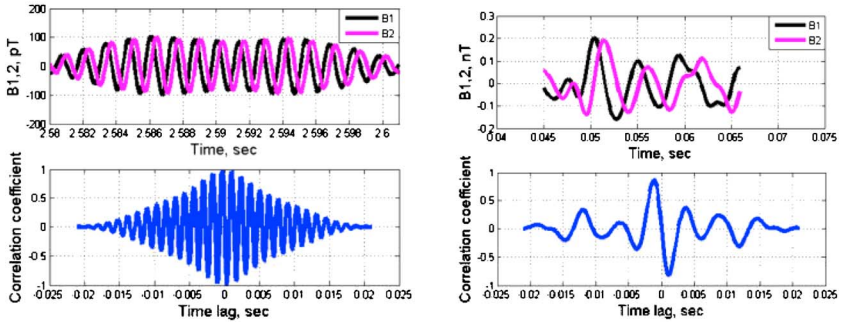

Figure 10. Coherency of a chorus subelement in the generation region in the left-hand panels and chorus quasi-coherency detected away from the generation region in the right-hand panels. The top two panels show the traces of the B1 and B2 minimum variance components, and the bottom panels the cross-correlation coefficients as functions of lag. Taken from *Tsurutani et al*. [2011b], their Figure A2.

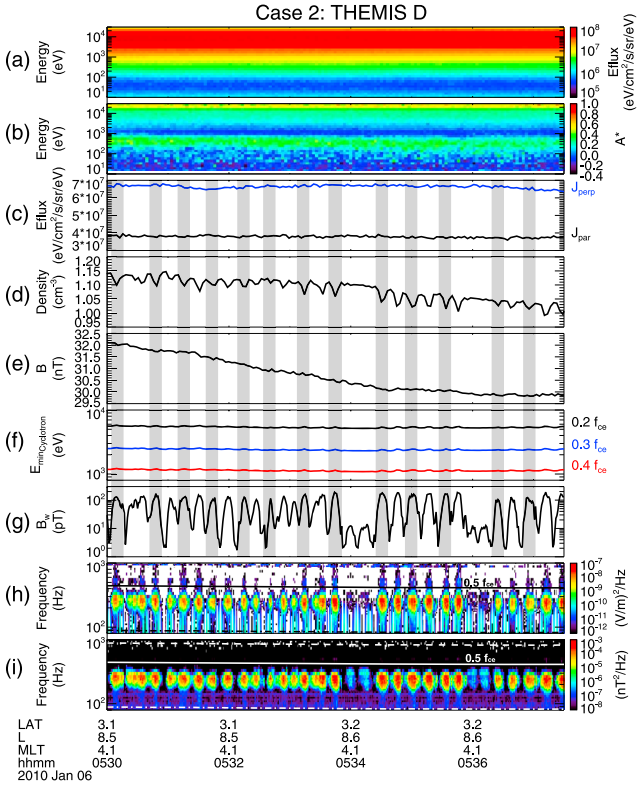

Figure 11. Outer zone chorus pulsations detected during 0530 to 0537:30 UT, 6 January 2010. (a, b) The omnidirectional electron energy flux and electron anisotropy. (c) The 3–30 keV electron energy perpendicular (blue) and parallel (black) to B_0. (d) The total electron density, (e) B_0, and (f) minimum resonant energy of electrons. (g) The integrated chorus wave amplitude from 0.05 to 0.5 Ω and 0.5 to 0.8 Ω. The spectrograms of the (h) wave electric and (i) magnetic fields, respectively. The figure was taken from *Li et al.* [2011c], their Figure 2.

electromagnetic waves had high cross-correlation values at large lags. On the other hand, chorus detected farther from the generation region (off-axis, away from the equator) were only quasi-coherent. The off-axis chorus lacked element and subelement temporal structures and were coherent over only one or two wave cycles.

[44] Figure 10 shows examples of these two different coherency cases. The top panels show the traces of the minimum variance [*Sonnerup and Cahill*, 1967; *Smith and Tsurutani*, 1976] B1 and B2 components (red and black traces) superposed on top of each other. In minimum variance coordinates, by convention, B1 and B2 are the maximum and intermediate variance components. Since chorus is a magnetically circularly polarized wave [*Verkhoglyadova et al.*, 2010], the two components have equal amplitudes separated by a phase angle of ~90°. The bottom left-hand panel illustrates the cross-correlation between these two components for a chorus subelement. The cross-correlation coefficient is ~1.0 at 90° lag (essentially zero lag) and then decreases to ~0.95 for ±1 wavelength lag. The right-hand panel shows an example of chorus detected farther away from the generation region. There were no clear chorus elements or subelements present for this case. The correlation coefficient between B1 and B2 are only ~0.8 for a phase lag of 90°, and this value decreases rapidly with increasing lag.

3.3. Microburst Formation by Coherent Wave-Particle Cyclotron-Resonant Interaction

[45] Many of the particle and bremsstrahlung X-ray observations discussed previously indicate that the pitch angle scattering process of electrons into the loss cone cannot be a slow diffusion associated with incoherent waves as assumed by *Kennel and Petschek* [1966] and *Tsurutani and Lakhina* [1997]. The *Lampton* [1967] observation of electron μBs appearing and disappearing on time scales of milliseconds and the *Anderson and Milton* [1964] observations of individual bremsstrahlung μB ~0.2 s pulses both strongly argue against such slow diffusion taking place. The partially filled loss cone identified by *Lee et al.* [2012] would also be difficult to explain.

[46] *Tsurutani et al.* [2009] suggested that if energetic ~10–100 keV electrons stayed in cyclotron resonance with parallel propagating chorus subelements for several or more wave cycles, there could be a rapid transport of the pitch angle of the electrons. Assuming the wave frequency to be ~800 Hz and a wave field of ~0.2 nT in a 125 nT dipole magnetic field strength, for a $V_{||} = c/3$ and interaction time of $\Delta t = 0.003$ s, a $\Delta\alpha = 7°$ would be achieved. An electron well outside of the loss cone could be "transported" into the center of the loss cone.

[47] *Lakhina et al.* [2010] constructed a wave-particle diffusion coefficient for these coherent waves. They derived the following expression:

$$D = \frac{B_\omega^2}{4B_0^2}\frac{\omega\Omega}{\left(\frac{\omega}{\Omega}+\frac{1}{2}\right)}\left[1+\frac{\omega\cos^2\varphi}{\Omega-\omega}\right]^2\tau \qquad (4)$$

where B_ω is the chorus wave magnetic field, φ is the angle between v⊥ and B_ω, ω is the wave frequency, and τ is the subelement duration. The above derivation implicitly assumes that the time duration of the chorus subelements, τ, is constant. In reality, the chorus subelements have time durations spanning a range of time periods from 1 ms to several hundreds of milliseconds. *Lakhina et al.* [2010] took a power law form of the distribution of the time durations, e.g., $P \propto \tau^{-\beta}$, where the spectral index β ranges between 1.5 and 3.0 [*Santolik et al.*, 2007], and P is the probability density. They derived a statistical pitch angle deviation (transport) of $\Delta\alpha$ ~2° to 20° for an interaction with one subelement and a $\langle D \rangle$ value of ~0.5 to 8.5 s^{-1}. Here the angular bracket denotes an average over chorus subelement time durations. This rapid pitch angle transport rate can explain the electron observations of *Lampton* [1967] and that of single μBs. Using the same values assuming the *Kennel and Petschek* [1966] and *Tsurutani and Lakhina* [1997] diffusion rate for scattering associated with incoherent waves, one gets a D of 3×10^{-2} s^{-1}, which is much too slow to explain μBs.

[48] *Tao et al.* [2012] have examined chorus amplitude modulation associated with chorus subelements and have shown from test particle code results that this could significantly affect the behavior of resonant electrons. The authors

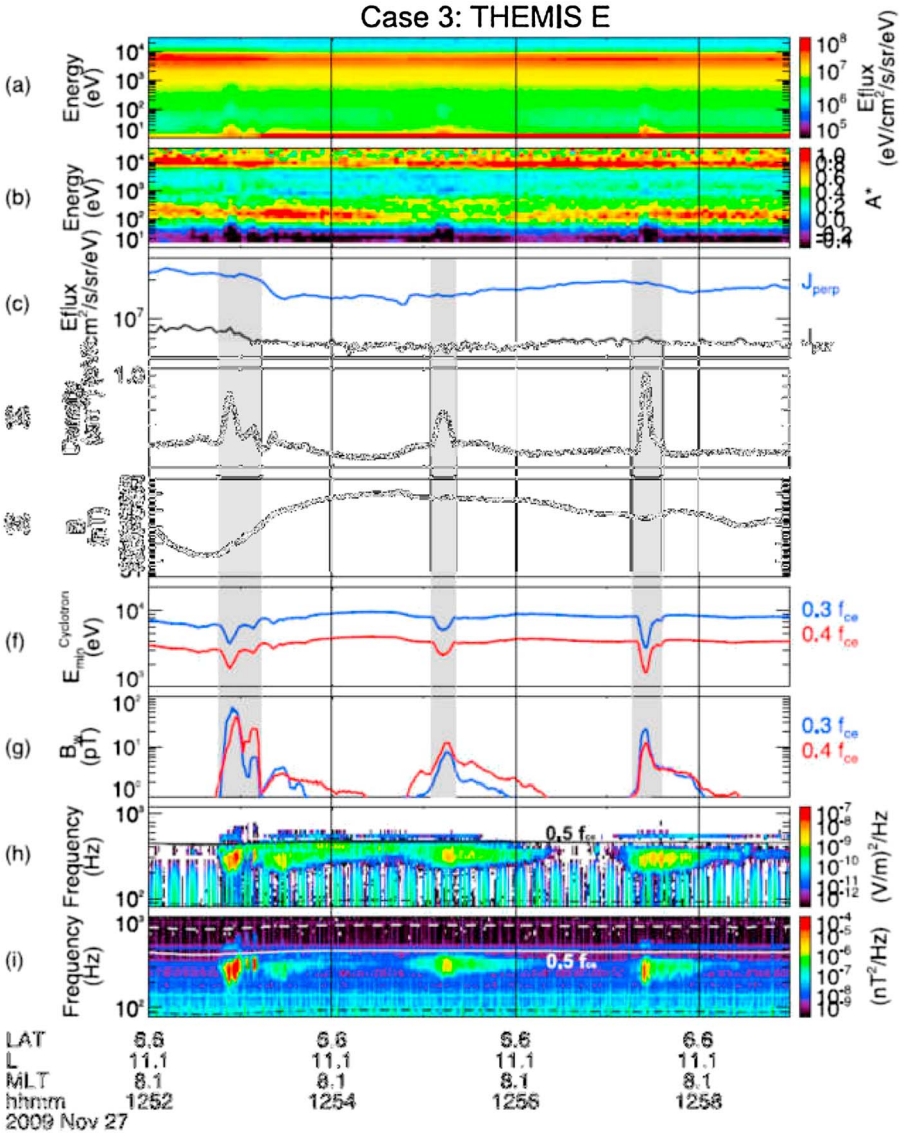

Figure 12. The same format as in Figure 11, but for THEMIS E at 1252 to 1259 UT. Figure 12f shows the minimum resonant electron energies for waves with 0.3 and 0.4 Ω. Figure 12g shows chorus wave amplitudes integrated over 0.25 to 0.35 Ω in blue and over 0.35 to 0.45 Ω in red. Taken from *Li et al.* [2011c], their Figure 4.

suggest that such amplitude modulation be considered in the quantitative treatment of electron-chorus interactions.

3.4. Chorus and Hiss 5–15 s Pulsations and Localized Plasma Density Enhancements/Decreases

[49] Some recent work by *Li et al.* [2011b, 2011c] using THEMIS wave, magnetometer, and plasma data have shed light on a possible mechanism for chorus and hiss generation and possibly pulsations. Li et al. have shown that magnetospheric chorus occurs in regions of both in situ plasma decreases and plasma increases. The plasma decreases are preferentially located in the midnight-to-dawn sector, and the density enhancements are preferentially located in the dawn-to-postnoon sector, although the authors note that there is a great deal of local time overlap between the density decreases and density increases. *Li et al.* [2011c] show that the density increases can lead to an intensification of chorus growth. This is much the same mechanism as that which leads to the general enhancement of chorus at dawn. However, they cautiously note that "other potential mechanisms for chorus intensification caused by density variations such as wave trapping by density crests and troughs cannot be excluded."

[50] Figure 11 shows an example of the *Li et al.* [2011c] results with chorus occurring in density decrease regions. This is a THEMIS *D* event that occurred at a morningside local time (~4.1 MLT) at a MLAT of ~3.2° and an L of ~8.5. A good example of this relationship is found from ~0534 to 0536 UT. In this interval, there are six consecutive density decreases (Figure 11d) associated with six bursts of chorus identified in the magnetic wave panel (Figure 11g). The quasi-periodicity between the chorus bursts are ~17 s. The plasma density decreases are coincident with the chorus bursts, so they also have ~17 s spacings. There are no

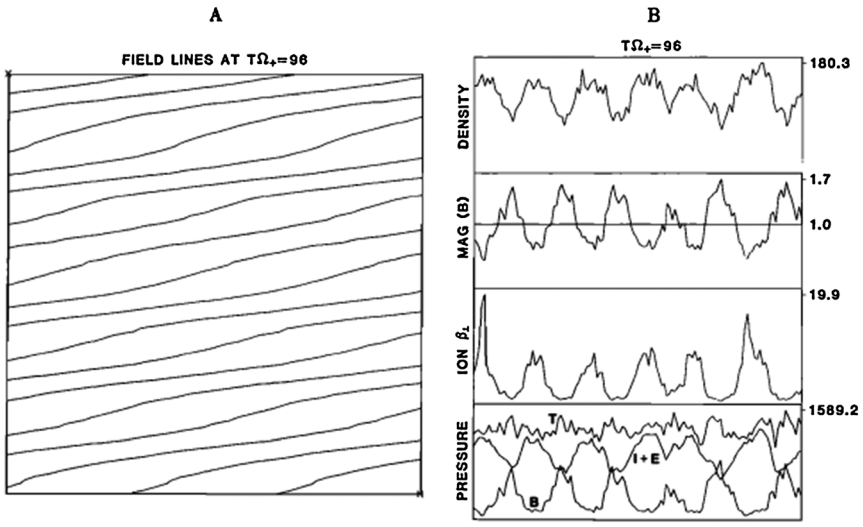

Figure 13. The left-hand panel shows the magnetic field lines from mirror instability simulation. The vertical axis (the simulation z axis) is along the wave vector direction. The horizontal axis (the simulation x axis) is perpendicular to the wave vector. The background magnetic field lies in the simulation *x-z* plane. The right-hand panel shows (from the top): the ion density, magnetic field magnitude, and the ion $\beta_{\perp}$. The bottom panel has three curves: the magnetic pressure (B), the ion plus electron thermal pressure (I + E), and the total pressure (T). The figure is taken from *Price et al*. [1986], their Figure 8.

obvious magnetic field magnitude (Figure 11e) variations associated with density decreases.

[51] Figure 12 shows chorus associated with plasma density increases. This event occurred from 1252 to 1259 UT on 27 November 2009. The event occurred in local morning hours (~8.1 MLT) at an L of ~11.1 [*Li et al*., 2011c]. There are three intervals of density enhancements indicated by gray shading. They are associated with the increase in <30 eV (thermal) electrons (Figure 12d). Chorus wave intensifications are well correlated with these density enhancements (Figures 12g, 12h, and 12i). These chorus bursts and density increases have spacings of ~135 s. There are no obvious magnetic magnitude variations (Figure 12e) associated with the density enhancements.

3.5. Chorus Wave Generation/Guidance by Mirror Mode Ducts?

[52] *Li et al*. [2011b] have suggested that these density enhancements and density depletions are associated with nonoscillatory mirror mode structures [*Chandrasekhar et al*., 1958; *Hasegawa*, 1969]. Li et al. mention that both density enhancements and depletions can lead to chorus generation but caution that wave guidance by these "ducts" is another possible source of the correlation between chorus and the density features.

[53] The magnetosphere is a low β plasma region, so it is possible that the magnetic field magnitude variations that are anticorrelated with plasma density variations for mirror mode structures detected in the magnetosheath [*Tsurutani et al*., 1982, 2011c] are difficult to discern. Mirror modes may be best detected primarily by the plasma properties inside the magnetosphere, as denoted by *Li et al*. [2011b].

[54] *Smith* [1961] and *Helliwell* [2006] have discussed electromagnetic wave trapping in both density depletion (troughs) and density enhancements (crests). Although the exact relationships for trapping depend on the density changes within the duct in comparison to the outside regions (a modest ~5–10% can be effective) and wave k angle, it is sufficient to say that trapping can occur for both density depletions and enhancements, given that the wave k is sufficiently parallel to the ambient magnetic field direction. *Helliwell* [2006] also noted that trapping of chorus for $f > 0.5$ Ω (upper band chorus) is only possible in density depletions.

[55] The reader should be reminded that the mirror instability generates both density enhancements and depletions not only on adjacent magnetic field lines but along the magnetic field as well. A two-dimensional picture showing this was generated by *Price et al*. [1986] and is shown as Figure 13. This simulation used a 1-D hybrid code, which assumed an ion beta of 2.5 for a range of values with $T_{\perp}/T_{\parallel} > 1$. For an ion temperature anisotropy of 1.5, the most unstable mirror waves propagated at ~74° relative to B_0. The most unstable wave had a wavelength of 14 r_p, where r_p is the proton gyroradius.

[56] In the figure, the lines represent magnetic field lines. In the left-hand panel areas where the magnetic field lines are close together, this represents high magnetic field strength regions. These areas are adjacent to regions where the lines are farther apart (low-intensity magnetic field regions). The panel also shows that along the magnetic field direction there are alternating high plasma density and low plasma density regions as well.

[57] In general, mirror mode regions are three-dimensional. Thus, there would be additional structures both into and out of the paper. Again, the high field regions would be adjacent to low field regions, and vice versa.

[58] The right-hand panel shows that the density (top curve) and magnetic field magnitude (second from the top) are 180° out of phase with each other. The total pressure (bottom panel, labeled "T") is constant. For more details concerning the parameters assumed for the simulation work, we refer the reader to the original article.

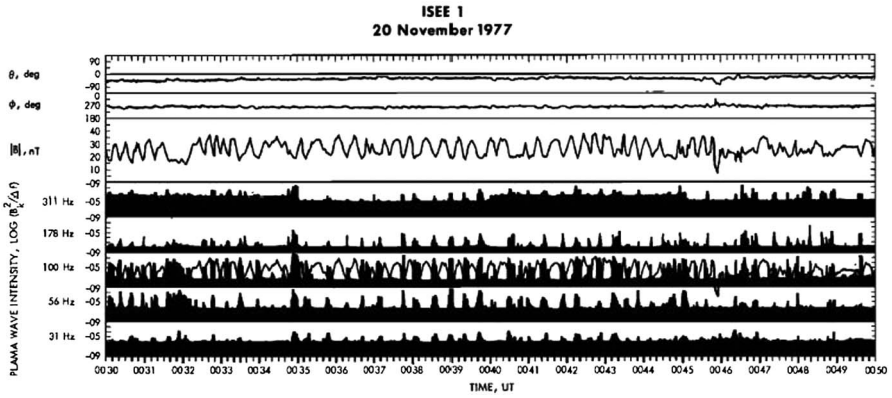

Figure 14. The relationship between lion roars and the high β portions (magnetic field decreases) of mirror modes. The top three panels are the field angles (in GSE coordinates) and the field magnitude. The lower channels are lion roar intensities in five spectral channels. The magnetic field magnitude is replotted in the ~100 Hz spectral channel for ease of visualization of the relationship between lion roars and the magnetic field decreases. Lion roars are detected at each and every field dip. The lion roars and mirror mode field dips have ~20 s spacings. This figure was taken from *Tsurutani et al*. [1982] their Figure 2.

3.6. Magnetosheath Lion Roars and Mirror Mode Structures

[59] We will briefly discuss electromagnetic whistler mode "lion roars" since their relationship to mirror mode structures seem to be quite similar to that of chorus' relationship to mirror modes. Lion roars were so named due to their sounds when played through a loudspeaker [*Smith et al*., 1967, 1971]. The emissions are short duration bursts with ~2 s durations and typical flat tone frequency-time characteristics [*Smith and Tsurutani*, 1976]. Packets of nearly monochromatic waves lasting a few cycles (~0.25 s) have been noted by *Baumjohann et al*. [1999]. These features are quite similar to chorus, except the time scales are a bit longer. The lion roar "elements" also do not have repetitive frequency-time structures, unlike chorus.

[60] Figure 14 shows the relationship between lion roars and local minima in magnetic field magnitudes (the high β regions) of mirror mode structures detected by the ISEE1 spacecraft. The lion roars are indicated by the dark regions of the five bottom panels. The magnetic field magnitude is superposed on the ~100 Hz spectral channel. It can be noted that lion roars occur in every one of the low field regions of the mirror mode structures. Since mirror modes in the magnetosheath are pressure balance structures [*Tsurutani et al*., 1982], this corresponds to high plasma density regions. This relationship is the same as that for chorus in Figure 12. To our knowledge, lion roars have not been detected in plasma density decreases (magnetic field increases) of mirror mode structures [see also *Zhang et al*., 1998]. Thus, a correlation such as that for chorus in Figure 11 has not been detected for magnetosheath lion roars.

[61] *Zhang et al*. [1998] have noted that in their Geotail study, lion roar waves propagate primarily in two directions, either along B_0 or in the anti-B_0 direction. The authors interpreted this to mean that the spacecraft was far from the generation region. Approximately 5% of the lion roars were noted to propagate in two opposite directions at the same time. The authors surmise that the spacecraft was in the local generation region at those times. *Zhang et al*. [1998] found that only ~30% of the lion roars studied were associated with mirror modes. The other 70% had no relationship to the magnetic dips or high β regions. An obvious interpretation is that lion roars are generated in the high β regions and then propagate away from those regions.

[62] Following the *Baumjohann et al*. [1999] work showing the coherency of lion roars, *Treumann et al*. [2000] suggested that the lion roars generated locally may be trapped within the mirror bottle, thus giving the coherent nature of the waves. These coherent waves are quite similar to chorus subelements.

4. Summary and Discussion

[63] 1. The temporal structure of chorus elements, ~5–15 s chorus groupings, are quite similar to that of μBs, μB trains, and 10–100 keV electron ~5–15 s pulsations. The *Kennel and Petschek* [1966] electron loss cone/temperature anisotropy instability is responsible for chorus/hiss generation. The *Lakhina et al*. [2010] theory assuming coherent chorus subelements can explain the extremely rapid pitch angle diffusion (transport) necessary for the millisecond time scale structure of μBs and singleton μBs. A normal Doppler-shifted cyclotron-resonant interaction at the equatorial plane is responsible for the electron pitch angle scattering and the loss of electrons to the ionosphere.

[64] 2. It is possible that ~5–15 s μB trains and ~5–15 s 10–100 keV electron precipitation pulsations are both caused by cyclotron-resonant wave-particle interactions with chorus and outer zone hiss. The former may be associated with groupings of chorus rising elements which are well separated from each other, whereas the latter are associated with falling-tone (overlapping) chorus or outer zone hiss emissions.

[65] 3. Relativistic μBs are most probably associated with chorus, at least during magnetic storm intervals. However, the nature of the chorus involved in the interactions at off-axis locations is still in question. Is the chorus there only

quasi-coherent, leading to a low pitch angle diffusion rate (leading to a partially filled loss cone), or can ducted chorus in mirror mode structures maintain wave coherency at off-axis locations and lead to more rapid diffusion rates? Perhaps both types of relativistic μBs exist in nature.

[66] 4. Do the mirror mode structures extend deeply along magnetic fields away from the equator and serve as ducts for chorus to reach the ground, particularly in the dawn local time region? Are these mirror mode structures the main source of ducts that allow chorus to reach the ground? What is the source of thermal ion temperature anisotropy that leads to the mirror instability? Further analyses will be necessary to answer these questions.

[67] 5. What is the mechanism for ~5–15 s μB trains and pulsations? Although the mirror mode structures were observed to have temporal spacings at about these same periods, this may be due to spatial rather than temporal structures. Chorus was detected in the high density regions (if total pressure is balanced, then these would correspond to high β regions) of the magnetospheric mirror mode structures as well as lion roars in the high β regions of magnetosheath mirror modes. Ionospheric ~5–15 s μB trains and ~5–15 s μB electron precipitation pulsations require that chorus/hiss is modulated with the above periods. The *Davidson* [1979] self-modulation mechanism should be tested by satellite ~10–100 keV electron data analyses and computer simulations.

[68] 6. The general separation of chorus rising tones and falling tones with local time is still generally unexplained. Why are the local time dependences different during solar maximum and solar minimum? The coherent chorus and lion roar subelements need to be theoretically explained in a unified fashion. A model applicable to all of the above observations should generally describe the lion roar flat tones as well as chorus rising and falling frequency elements.

[69] 7. If wave-particle interactions involving chorus and >1 MeV electrons are responsible for relativistic μBs, relativistic μB trains and relativistic ~5–15 s pulsations are also expected to occur in nature. To our knowledge, these phenomena have not yet been detected.

[70] 8. If ~10 to 100 ms coherent chorus subelements are responsible for fast pitch angle transport of ~10–100 keV electrons into the loss cone, then μB substructure should be present and observable under ideal conditions.

[71] 9. What is the cause of the coherent nature of chorus subelements? Can the *Treumann et al*. [2000] mechanism for lion roar coherency be somehow applied to the magnetic equatorial region?

5. Final Comments

[72] We have attempted to give the reader a brief review of some of the major features of ~10 to 100 keV electron precipitation and waves that cause their pitch angle scattering into the loss cone. This scattering results in the observed μBs, μB trains, ~5–15 s X-ray pulsations, optical pulsations, and relativistic μBs.

[73] In our review, we have cited the first publications of important findings, which were felt to be the most important ones. Otherwise, these references may eventually get lost, and these physical features will get "rediscovered" at some later date. We note that this has already happened for some of the earlier works (1960s) cited here. We hope we did an accurate and adequate job in this area. We did not attempt to give a complete reference list concerning the important physical features of μBs and chorus. To do so would have required an enormous effort and the expansion of the reference list by perhaps a factor of 10. We apologize for this omission.

[74] We have attempted to indicate where our knowledge is presently limited, hoping that the interested reader will perform future research in order to give further clarity to the microphysics of ~10–100 keV electron loss processes. This is perhaps the most useful part of this review. It is our hope that the BARREL [*Millan and The BARREL team*, 2011] and the Van Allen Probes (formerly called the Radiation Belt Storm Probes or RBSP: *Mauk et al*. [2012]) missions will answer most of the fundamental outstanding questions in addition to making new discoveries.

Appendix A: Two-Frequency Bands of Chorus

[75] The 10–100 keV microburst precipitation have been ascribed to be due to resonant interactions with the lower frequency band of two-frequency chorus. Here we present some background material concerning the two bands and their frequency separation for the interested reader.

[76] Figures 7 and 8 both showed two bands of chorus, occurring at different frequencies. In Figure 7, there were structureless ~5 to 15 s quasi-periodic hiss emissions extending from ~300 to ~500 Hz, which were followed in time by higher frequency chorus overlapping falling tones at ~700 to ~850 Hz. In Figure 8, there are hiss bands extending from ~200 Hz to ~500 Hz, followed by higher frequency chorus structures from ~600 to ~750 Hz. In both of these cases, the "gap" between the two-frequency bands spans 0.5 Ω_{eq}, where Ω_{eq} is the electron cyclotron frequency at the magnetic equator. Figure A1 shows an early OGO5 analysis of midnight sector chorus and their frequency ranges.

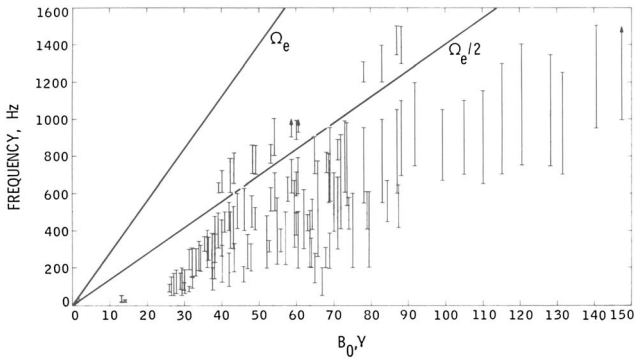

Figure A1. The frequency range of midnight sector chorus, normalized to the magnetic field at the equatorial plane. Solid lines correspond to Ω_{eq} and $\Omega_{eq}/2$. Most chorus span a range from 0.1 to <0.5 Ω_{eq}. In some cases, another band also exists from >0.5 to ~0.7 Ω_{eq}. Bands of >0.5 Ω_{eq} alone were rarely detected. Taken from *Tsurutani and Smith* [1974], their Figure 7.

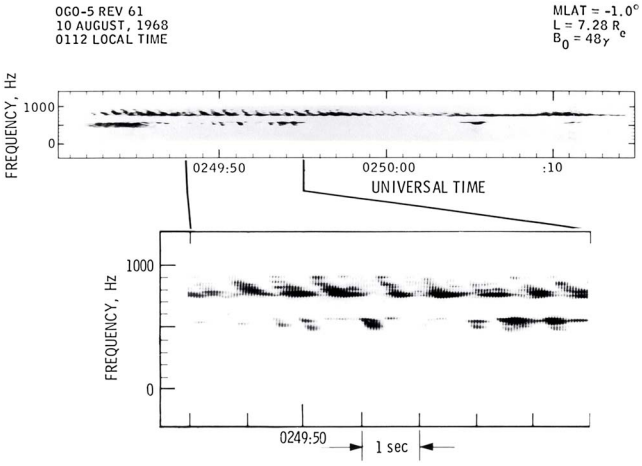

Figure A2. Two-frequency falling-tone chorus bounding a gap at ~0.5 Ω_{eq}. Taken from *Tsurutani and Smith* [1974], their Figure 4.

[77] Figure A1 shows the frequency range of midnight sector chorus normalized to the magnetic field magnitude at the magnetic equator. There are two different frequency ranges, one below 0.5 Ω_{eq} (called lower band chorus) and a second above 0.5 Ω_{eq} (called upper band chorus). There are no emissions that occur exactly at 0.5 Ω_{eq}. All cases where upper band chorus occurred were cases where lower band chorus was also present.

[78] Although Figures 7 and 8 showed cases where the two bands of chorus were seemingly unrelated (although in Figure 7 each hiss pulsation was followed by a band of higher frequency falling-tone chorus, thus there clearly is some causal relationship between the first emissions and the following), there are cases where the chorus in the upper band and the lower band are more clearly related.

[79] Figure A2 shows an example of two-frequency falling-tone chorus. The example was taken at 0112 LT, at an L of ~7.3 and an MLAT of −1.0. The lower band of chorus extends from ~440 to 540 Hz, and the upper band from ~710 to 900 Hz. The gap from 540 to 710 Hz corresponds to 0.40 to 0.52 Ω_{eq}. In the insert, the upper and lower band falling tones appear to be connected except for the gap. In their OGO5 survey, *Tsurutani and Smith* [1974] noted that not all two-frequency chorus had gaps at 0.5 Ω_{eq}. About 10% of the cases had gaps at frequencies outside of 0.5 Ω_{eq}.

[80] The gap of two-frequency chorus at ~0.5Ω_{eq} was thought to be due to Landau damping by *Tsurutani and Smith* [1974] and *Coroniti et al*. [1984]. *Omura et al*. [2009] have attempted to explain the gap by nonlinear damping of slightly obliquely propagating chorus along inhomogeneous ambient magnetic fields.

[81] Figure A3 shows the distribution of OGO5 two-frequency chorus occurrence. L from 4 to 15 are given as a radius and MLT as the azimuth angle. Midnight (0 MLT) is at the bottom and dawn (06 MLT) at the right. Two-frequency chorus shows the approximately same spatial distribution as that of low-frequency chorus. There is enhancement near local midnight with higher occurrence frequency postdawn. There is a paucity of two-frequency chorus in the afternoon-to-midnight sector. The highest occurrence frequency in this survey was 15–18% (see legend). A similar MLT-L distribution of the upper frequency chorus has been noted by *Li et al*. [2011d].

[82] A long-standing question about two-frequency chorus has been "What mechanism is responsible for the upper band chorus?" Generation of the lower band is clear and has been discussed already. Recent results from *Li et al*. [2012b] indicate that high thermal plasma densities lead to hiss-like chorus. Another result from *Li et al*. [2011d] is that (some) upper band chorus propagates at highly oblique angles and thus may be generated by a different mechanism than that for lower band chorus. We therefore revisit Figures 7 and 8 in this light. In these cases, hiss-like chorus is followed by upper band chorus. We know that the lower band chorus will pitch angle scatter the ~10–100 keV

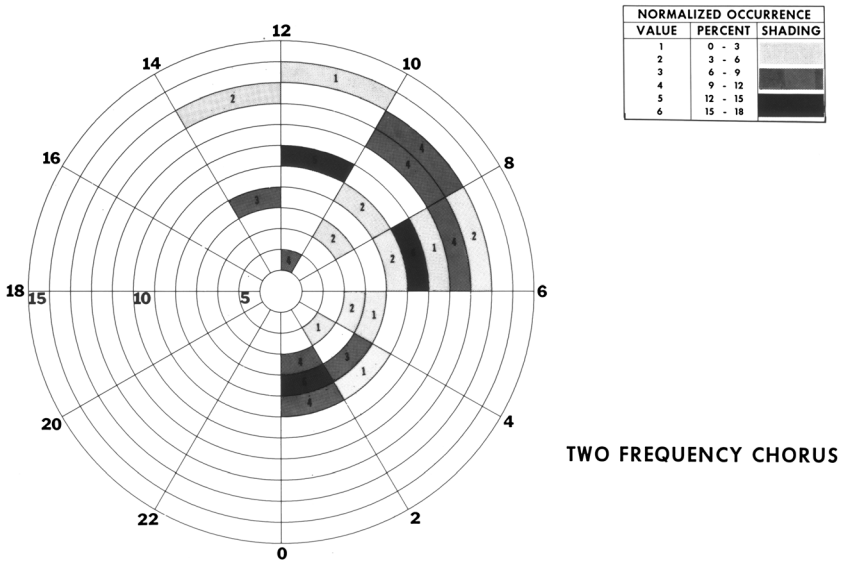

Figure A3. The MLT and L distribution of two-frequency chorus. The distribution is the same as for the regular distribution of low-frequency chorus.

electrons (relaxing the temperature anisotropy), filling the loss cone. The loss cone electron beam will run through the high density plasma. These electrons could generate upper band chorus via a Cherenkov radiation mechanism. The two-frequency chorus shown in Figure A2 is different, however. The lower band emission is composed of discrete falling tones. The tones below the $\Omega_{eq}/2$ gap and above the gap seem to be related. Thus, for this case, it is possible that both bands are generated by the temperature anisotropy/loss cone instability. The anisotropic electrons might be in a lower energy range of ~5 to 20 keV in order to accommodate the high-frequency emission. Such phenomena would be expected in the outer regions of the magnetosphere where compression from magnetospheric convection was weaker. Such was the case for that particular event. These ideas can be easily tested by observations on the Van Allen Probes and modeling work. It will be interesting to find out if there is only one mechanism or two in the generation of upper band chorus.

[83] **Acknowledgments.** This work is dedicated to the late Kinsey A. Anderson, who with his coworkers and former students did much to advance our understanding of microburst physics. Portions of this research were performed at the Jet Propulsion Laboratory, California Institute of Technology, under contract with the National Aeronautics and Space Administration. B.T.T. thanks P. Bellan and Cal. Tech. for hosting him during a sabbatical leave. G.S.L. thanks the Indian National Science Academy, New Delhi, for support under the Senior Scientist Scheme.

[84] Robert Lysak thanks the reviewers for their assistance in evaluating this paper

References

Anderson, K. A. (1958), Soft radiation events at high altitude during the magnetic storm of August 29–30, 1957, *Phys. Rev.*, *111*(5), 1397.

Anderson, K. A., and D. W. Milton (1964), Balloon observation of X-rays in the auroral zone III, high time resolution studies, *J. Geophys. Res.*, *69*, 4457.

Anger, C. D., J. R. Barcus, R. R. Brown, and D. S. Evans (1963), Auroral zone X-ray pulsations in the 1- to 15-second period range, *J. Geophys. Res.*, *68*, 1023.

Banks, P. M., and T. E. Holzer (1968), The polar wind, *J. Geophys. Res.*, *73*, 6846.

Barcus, J. R., and A. Christensen (1965), A 75-second periodicity in auroral zone X Rays, *J. Geophys. Res.*, *70*, 5455.

Barcus, J. R., and T. J. Rosenberg (1965), Observations on the spatial structure of pulsating electron precipitation accompanying low frequency hydromagnetic disturbances in the auroral zone, *J. Geophys. Res.*, *70*, 1707.

Barcus, J. R., R. R. Brown, and T. J. Rosenberg (1966), Spatial and temporal character of fast variations in auroral zone X-rays, *J. Geophys. Res.*, *71*, 125.

Barcus, J. R., R. R. Brown, R. H. Karas, T. J. Rosenberg, H. Trefall, and K. Bronstad (1971), Auroral X-ray pulsations in the 1.2- to 4-second period range, *J. Geophys. Res.*, *76*, 3811.

Baumjohann, W., R. A. Treumann, E. Georgescu, G. Haerendel, K.-H. Fornacon, and U. Auster (1999), Waveform and packet structure of lion roars, *Ann. Geophys.*, *17*, 1528.

Bell, T. F., and O. Buneman (1964), Plasma instability in the whistler mode caused by a gyrating electron stream, *Phys. Rev.*, *133*(5A), 25.

Bortnik, J., and R. M. Thorne (2007), The dual role of ELF/VLF chorus waves in the acceleration and precipitation of radiation belt electrons, *J. Atmos. Sol.-Terr. Phys.*, *69*, 378.

Brekke, A. (1971), On the correlation between pulsating aurora and cosmic radio noise absorption, *Planet. Space Sci.*, *19*, 891.

Brice, N. (1963), An explanation of triggered very-low-frequency emissions, *J. Geophys. Res.*, *68*, 4626.

Brice, N. (1964a), A quantitative explanation of the diurnal variation of chorus, *J. Geophys. Res.*, *69*, 4701.

Brice, N. (1964b), Fundamentals of very low frequency emission generation mechanisms, *J. Geophys. Res.*, *69*, 4515.

Brice, N., and C. Lucas (1971), Influence of magnetospheric convection and polar wind on loss of electrons from the outer radiation belt, *J. Geophys. Res.*, *76*, 900.

Brown, R. R., J. R. Barcus, and N. R. Parsons (1965), Balloon observations of auroral zone X-rays in conjugate regions, 2. Microbursts and pulsations, *J. Geophys. Res.*, *70*, 2599.

Burtis, W. J., and R. A. Helliwell (1969), Banded chorus—A new type of VLF radiation observed in the magnetosphere by Ogo 1 and Ogo 3, *J. Geophys. Res.*, *74*, 3002.

Burtis, W. J., and R. Helliwell (1976), Magnetospheric chorus: Occurrence patterns and normalized frequency, *Planet. Space Sci.*, *24*(11), 1007, doi:10.1016/0032-0633(76)90119-7.

Chandrasekhar, S., A. M. Kaufman, and K. M. Watson (1958), The stability of the pinch, *Proc. R. Soc. London, Ser. A*, *245*(435), doi:10.1098/rspa.1958.0094.

Coroniti, F. V., and C. F. Kennel (1970a), Electron precipitation pulsations, *J. Geophys. Res.*, *75*, 1279.

Coroniti, F. V., and C. F. Kennel (1970b), Auroral micropulsation instability, *J. Geophys. Res.*, *75*, 1863.

Coroniti, F. V., F. L. Scarf, C. F. Kennel, and W. S. Kurth (1984), Analysis of chorus emissions at Jupiter, *J. Geophys. Res.*, *89*(A6), 3801.

Cresswell, G. R., and T. N. Davis (1965), Observations on pulsating auroras, *Goddard Space Flt Cent. X-612-65-485*, Greenbelt Maryland.

Davidson, G. T. (1979), Self-modulated VLF wave-electron interactions in the magnetosphere: A cause of auroral pulsations, *J. Geophys. Res.*, *84*, 6517.

DeForest, S. E., and C. E. McIlwain (1971), Plasma clouds in the magnetosphere, *J. Geophys. Res.*, *76*, 3587.

Goldstein, B. E., and B. T. Tsurutani (1984), Wave normal directions of chorus near the equatorial source region, *J. Geophys. Res.*, *89*(A5), 2789.

Gonzalez, W. D., J. A. Joselyn, Y. Kamide, H. W. Kroehl, G. Rostoker, B. T. Tsurutani, and V. M. Vasyliunas (1994), What is a geomagnetic storm?, *J. Geophys. Res.*, *99*(A4), 5771.

Gurnett, D. A., and B. J. O'Brien (1964), High-latitude geophysical studies with satellite Injun 3, 5. Very-low-frequency electromagnetic radiation, *J. Geophys. Res.*, *69*, 65, doi:10.1029/JZ069i001p00065.

Hartz, T. R., and N. M. Brice (1967), The general pattern of auroral particle precipitation, *Plan. Space Sci.*, *15*(2), 301.

Hasegawa, A. (1969), Drift mirror instability in the magnetosphere, *Phys. Fluids*, *12*, 2642, doi:10.10.1063/1.1692407.

Hayakawa, M., K. Ohta, and S. Shimakura (1990), Spaced direction finding of nighttime whistlers at low and equatorial latitudes and their propagation mechanism, *J. Geophys. Res.*, *95*(A9), 15091, doi:10.1029/JA095iA09p15091.

Helliwell, R. A. (2006), *Whistlers and Related Ionospheric Phenomena*, pp. 43, 203, Dover Publ, Mineola, New York.

Horne, R. B., and R. M. Thorne (1998), Potential waves for relativistic electron scattering and stochastic acceleration during magnetic storms, *Geophys. Res. Lett.*, *25*(15), 3011.

Horne, R. B., and R. M. Thorne (2003), Relativistic electron acceleration and precipitation during resonant interactions with whistler-mode chorus, *Geophys. Res. Lett.*, *30*(10), 1527, doi:10.1029/2003GL01673.

Imhof, W. L., H. D. Voss, J. Mobilia, D. W. Datlowe, E. E. Gaines, J. P. McGlennon, and U. S. Inan (1992), Relativistic electron microbursts, *J. Geophys. Res.*, *97*, 13829.

Inan, U. S., T. F. Bell, and R. A. Helliwell (1978), Nonlinear pitch angle scattering of energetic electrons by coherent VLF waves in the magnetosphere, *J. Geophys. Res.*, *83*, 3235.

Isted, G. A., and G. Millington (1957), The "dawn chorus" in radio observations, *Nature*, *180*, 716.

Jentsch, V. (1976), Electron precipitation in the morning sector of the auroral zone, *J. Geophys. Res.*, *81*, 135.

Johansen, O. E., and A. Omholt (1966), A study of pulsating aurora, *Planet Space Sci.*, *14*, 207.

Kennel, C. F., and H. E. Petschek (1966), Limit on stably trapped particle fluxes, *J. Geophys. Res.*, *71*, 1.

Lakhina, G. S., B. T. Tsurutani, O. P. Verkhoglyadova, and J. S. Pickett (2010), Pitch angle transport of electrons due to cyclotron interactions with coherent chorus subelements, *J. Geophys. Res.*, *115*, A00F15, doi:10.1029/2009JA014885.

Lampton, M. (1967), Daytime observations of energetic auroral-zone electrons, *J. Geophys. Res.*, *72*, 5817.

Lauben, D. S., U. S. Inan, T. F. Bell, and D. A. Gurnett (2002), Source characteristics of ELF/VLF chorus, *J. Geophys. Res.*, *107*(A12), 1429, doi:10.1029/2000JA003019.

LeDocq, M. J., D. A. Gurnett, and G. B. Hospodarsky (1998), Chorus source locations from VLF Poynting flux measurements with the Polar spacecraft, *Geophys. Res. Lett.*, *25*, 4063, doi:10.1029/1998GL90071.

Lee, J. J., G. K. Parks, E. S. Lee, B. T. Tsurutani, J. Hwang, K. S. Cho, K.-H. Kim, Y. D. Park, K. W. Min, and M. P. McCarthy (2012),

Anisotropic pitch angle distribution of ~100 keV microburst electrons in the loss cone: Measurements from STSAT-1, *Ann. Geophys.*, *30*, 1567.

Lessard, M. R. (2012), A review of pulsating aurora, in *Auroral Phenomenology and Magnetospheric Processes: Earth and Other Planets*, Geophys. Mon. Ser., *197*, edited by A. Keiling et al., 55pp., AGU., Washington, D.C., doi:10.1029/2011GM00187.

Li, W., R. M. Thorne, J. Bortnik, Y. Y. Shprits, Y. Nishimura, V. Angelopoulos, C. Chaston, O. Le Contel, and J. W. Bonnell (2011a), Typical properties of rising and falling tone chorus waves, *Geophys. Res. Lett.*, *38*, L14103, doi:10.1029/2011GL047925.

Li, W., R. M. Thorne, J. Bortnik, Y. Nishimura, and V. Angelopoulos (2011b), Modulation of whistler mode chorus waves: 1. Role of compressional Pc4-5 pulsations, *J. Geophys. Res.*, *116*, A06205, doi:10.1029/2010JA016312.

Li, W., J. Bortnik, R. M. Thorne, Y. Nishimura, V. Angelopoulos, and L. Chen (2011c), Modulation of whistler mode chorus waves: 2. Role of density variations, *J. Geophys. Res.*, *116*, A06206, doi:10.1029/2010JA016313.

Li, W., J. Bortnik, R. M. Thorne, and V. Angelopoulos (2011d), Global distribution of wave amplitudes and wave normal angles using THEMIS wave observations, *J. Geophys. Res.*, *116*, A12205, doi:10.1029/2011JA017035.

Li, W., J. Bortnik, Y. Nishimura, R. M. Thorne, and V. Angelopoulos (2012a), The origin of pulsating aurora: Modulated whistler mode chorus waves, in *Auroral Phenomenology and Magnetospheric Processes: Earth and Other Planets*, Geophys. Mon. Ser., *197*, edited by A. Keiling et al., p. 379, AGU, Washington, D.C., doi:10.1029/2011GM001164.

Li, W., R. M. Thorne, J. Bortnik, X. Tao, and V. Angelopoulos (2012b), Characteristics of hiss-like and discrete whistler-mode emissions, *Geophys. Res. Lett.*, *39*, L18106, doi:10.1029/2012GL053206.

Lorentzen, K. R., M. D. Looper, and J. B. Blake (2001a), Relativistic electron microbursts during the GEM storms, *Geophys. Res. Lett.*, *28*, 2573.

Lorentzen, K. R., J. B. Blake, U. S. Inan, and J. Bortnik (2001b), Observation of relativistic electron microbursts in association with VLF chorus, *J. Geophys. Res.*, *106*, 6017.

Mauk, B. H., N. J. Fox, S. G. Kanekal, R. L. Kessel, D. G. Sibeck, and A. Ukhorskiy (2012), Science objectives and rationale for the Radiation Belt Storm Probes mission, *Space Sci. Rev.*, doi:10.1007/s11214-012-9908-y.

Millan, R. M., and The BARREL team (2011), Understanding relativistic electron losses with BARREL, *J. Atmos. Sol.-Terr. Phys.*, *73*, 1425.

Nakamura, R., M. Isowa, Y. Kamide, D. N. Baker, J. B. Blake, and M. Looper (2000), SAMPEX observations of precipitation bursts in the outer radiation belt, *J. Geophys. Res.*, *105*, 15875.

Nishimura, Y. et al. (2010), Identifying the driver of pulsating auroras, *Science*, *330*, 81.

Nishimura, Y., et al. (2011), Multievent study of the correlation between pulsating auroras and whistler mode chorus emissions, *J. Geophys. Res.*, *116*, A11221, doi:10.1029/2011JA016876.

Nunn, D. (1974), A self-consistent theory of triggered VLF emissions, *Planet. Space Sci.*, *22*, 349.

Nunn, D., and Y. Omura (2012), A computational and theoretical analysis of falling frequency VLF emissions, *J. Geophys. Res.*, *117*, A08228, doi:10.1029/2012JA017557.

Oguti, T. (1976), Recurrent auroral patterns, *J. Geophys. Res.*, *81*, 1782.

Oguti, T., K. Hayashi, T. Yamamoto, J. Ishida, T. Higuchi, and N. Nishitani (1986), Absence of hydromagnetic waves in the magnetospheric equatorial region conjugate with pulsating auroras, *J. Geophys. Res.*, *91*, 13,711.

Omura, Y., Y. Katoh, and D. Summers (2008), Theory and simulation of the generation of whistler-mode chorus, *J. Geophys. Res.*, *113*, A04223, doi:10.1029/2007JA012622.

Omura, Y., M. Hikishima, Y. Katoh, D. Summers, and S. Yagitani (2009), Nonlinear mechanisms of lower-band and upper-band VLF chorus emissions in the magnetosphere, *J. Geophys. Res.*, *114*, A07217, doi:10.1029/2009JA014206.

Parks, G. K. (1967), Spatial characteristics of auroral-zone X-ray microbursts, *J. Geophys. Res.*, *72*, 215.

Price, C. P., D. W. Swift, and L.-C. Lee (1986), Numerical simulation of nonoscillatory mirror mode waves at the Earth's magnetosheath, *J. Geophys. Res.*, *91*, 101, doi:10.1029/JA091iA01p00101.

Rosenberg, T. J., J. Bjordal, and G. J. Kvifte (1967), On the coherency of X-ray and optical pulsations in auroras, *J. Geophys. Res.*, *72*, 3504.

Rosenberg, T. J., R. A. Helliwell, and J. P. Katsufrakis (1971), Electron precipitation associated with discrete very-low-frequency emissions, *J. Geophys. Res.*, *76*, 8445.

Russell, C. T., R. E. Holzer, and E. J. Smith (1969), Ogo 3 observations of ELF noise in the magnetosphere, 1, Spatial extent and frequency of occurrence, *J. Geophys. Res.*, *74*, 755.

Saito, S., Y. Miyoshi, and K. Seki (2012), Relativistic electron microbursts associated with whistler chorus rising tone elements: GEMSIS-RBW simulations, *J. Geophys. Res.*, *117*, A10206, doi:10.1029/2012JA018020.

Sandahl, I., L. Eliasson, and R. Lundin (1980), Rocket observations of precipitating electrons over a pulsating aurora, *Geophys. Res. Lett.*, *7*, 309.

Santolik, O., D. A. Gurnett, J. S. Pickett, M. Parrot, and N. Cornilleau-Wehrlin (2003), Spatio-temporal structure of storm-time chorus, *J. Geophys. Res.*, *108*(A7), 1278, doi:10.1029/2002JA009791.

Santolik, O., D. A. Gurnett, J. S. Pickett, M. Parrot, and N. Cornilleau-Wehrlin (2004), A microscopic and nanoscopic view of storm-time chorus on 31 March, 2001, *Geophys. Res. Lett.*, *31*, L02801, doi:10.1029/2003GL018757.

Santolik, O., D. A. Gurnett, and J. S. Pickett (2007), Observations of very high amplitudes of whistler-mode chorus: Consequences for nonlinear trapping of energetic electrons in the outer radiation belt, *Eos Trans. Trans*., AGU, *88*, abstract SM14B-07.

Scourfield, M. W. J., and N. R. Parsons (1971), Pulsating auroral patches exhibiting sudden intensity-dependent spatial expansion, *J. Geophys. Res.*, *76*, 4518.

Scourfield, M. W. J., G. R. Cresswell, G. R. Pilkington, and N. R. Parsons (1970), Auroral pulsations—Television image and X-ray correlations, *Planet. Space Sci.*, *18*, 495.

Smith, R. L. (1961), Propagation characteristics of whistlers trapped in field-aligned columns of enhanced ionization, *J. Geophys. Res.*, *66*, 3699.

Smith, E. J., and B. T. Tsurutani (1976), Magnetosheath lion roars, *J. Geophys. Res.*, *81*, 2261, doi:10.1029/JA081i013p02261.

Smith, E. J., R. E. Holzer, and C. T. Russell (1967), Magnetic emissions in the magnetosheath at frequencies near 100 Hz, *J. Geophys. Res.*, *74*, 4803.

Smith, E. J., A. M. A. Frandsen, and R. E. Holzer (1971), Lion roars in the magnetosheath (abstract), *Eos Trans. AGU*, *52*, 903.

Sonnerup, B. U., and L. J. Jr.Cahill (1967), Magnetopause structure and attitude from Explorer 12 observations, *J. Geophys. Res.*, *72*, 171, doi:10.1029/JZ072i001p00171.

Storey, L. R. O. (1953), An investigation of whistling atmospherics, *Phil. Trans. Roy. Soc.*, *246*, 113.

Sudan, R. N. (1963), Plasma electromagnetic instabilities, *Phys. Fluids*, *6*, 57.

Tao, X., J. Bortnik, R. M. Thorne, J. M. Albert, and W. Li (2012), Effects of amplitude modulation on nonlinear interactions between electrons and chorus waves, *Geophys. Res. Lett.*, *39*, L06102, doi:10.1029/2012GL051202.

Thorne, R. M., T. P. O'Brien, Y. Y. Shprits, D. Summers, and R. B. Thorne (2005), Timescale for MeV electron microburst loss during geomagnetic storms, *J. Geophys. Res.*, *110*, A09202, doi:10.1029/2004JA010882.

Treumann, R. A., E. Georgescu, and W. Baumjohann (2000), Lion roar trapping in mirror modes, *Geophys. Res. Lett.*, *27*, 1843.

Tsurutani, B. T., and E. J. Smith (1974), Postmidnight chorus: A substorm phenomenon, *J. Geophys. Res.*, *79*, 118.

Tsurutani, B. T., and E. J. Smith (1977), Two types of magnetospheric ELF chorus and their substorm dependences, *J. Geophys. Res.*, *82*, 5112.

Tsurutani, B. T., and G. S. Lakhina (1997), Some basic concepts of wave-particle interactions in collisionless plasmas, *Rev. Geophys.*, *35*, 491.

Tsurutani, B. T., E. J. Smith, H. I. West, Jr., and R. M. Buck (1979), Chorus, energetic electrons and magnetospheric substorms, in *Wave Instabilities in Space Plasmas*, edited by P. J. Palmadesso, and K. Papadopoulos, 55pp., D. Reidel.

Tsurutani, B. T., E. J. Smith, R. R. Anderson, K. W. Ogilvie, J. D. Scudder, D. N. Baker, and S. J. Bame (1982), Lion roars and nonoscillatory drift mirror waves in the magnetosheath, *J. Geophys. Res.*, *87*, 6060, doi:10.1029/JA087iA08p06060.

Tsurutani, B. T., O. P. Verkhoglyadova, G. S. Lakhina, and S. Yagitani (2009), Properties of dayside outer zone chorus during HILDCAA events: Loss of energetic electrons, *J. Geophys. Res.*, *114*, A03207, doi:10.1029/2008JA013353.

Tsurutani, B. T., E. Echer, and W. D. Gonzalez (2011a), The solar and interplanetary causes of the recent minimum in geomagnetic activity (MGA23): A combination of midlatitude small coronal holes, low IMF Bz variances, low solar wind speeds and low solar magnetic fields, *Ann. Geophys.*, *29*, 1, doi:10.5194/angeo-29/1/2011.

Tsurutani, B. T., B. J. Falkowski, O. P. Verkhoglyadova, J. S. Pickett, O. Santolik, and G. S. Lakhina (2011b), Quasi-coherent chorus properties: 1. Implications for wave-particle interactions, *J. Geophys. Res.*, *116*, A09210, doi:10.1029/2010JA016237.

Tsurutani, B. T., G. S. Lakhina, O. P. Verkhoglyadova, E. Echer, F. L. Guarnieri, Y. Narita, and D. O. Constantinescu (2011c), Magnetosheath and heliosheath mirror mode structures, interplanetary magnetic decreases, and linear magnetic decreases: Differences and distinguishing features, *J. Geophys. Res.*, *116*, A02103, doi:10.1029/2010JA015913.

Van Allen, J. A. (1995), Early rocket observations of auroral bremsstrahlung and its absorption in the mesosphere, *J. Geophys. Res.*, *100*, 14,485.

Verkhoglyadova, O. P., B. T. Tsurutani, and G. S. Lakhina (2010), Properties of obliquely propagating chorus, *J. Geophys. Res.*, *115*, A00F19, doi:10.1029/2009JA014809.

Winckler, J. R., L. Peterson, R. Arnoldy, and R. Hoffman (1958), X-rays from visible aurorae at Minneapolis, *Phys. Rev.*, *110*(6), 1221.

Winckler, J. R., L. Peterson, R. Hoffman, and R. Arnoldy (1959), Auroral X-rays, cosmic rays, and related phenomena during the storm of February 10–11, 1958, *J. Geophys. Res.*, *64*, 597.

Winckler, J. R., P. D. Bhavsar, and K. A. Anderson (1962), A study of the precipitation of energetic electrons from the geomagnetic field during magnetic storms, *J. Geophys. Res.*, *67*, 3717.

Yamamoto, T. (1988), On the temporal fluctuations of pulsating auroral luminosity, *J. Geophys. Res.*, *93*, A2, 897.

Zhang, Y., H. Matsumoto, and H. Kojima (1998), Lion roars in the magnetosheath: The Geotail observations, *J. Geophys. Res.*, *103*, 4615.